Numerical Modeling of Seismic Wave Propagation at the Micro-Scale in Digitized Sandstone

Yang Zhang, Fuxian Song, M.Nafi Toksöz

Earth Resources Laboratory
Dept. of Earth, Atmospheric and Planetary Sciences
Massachusetts Institute of Technology
Cambridge, MA 02139

Abstract

In this paper, we first examine the relationship between the relative particle motions of fluids and solids and the seismic signal received when compressional waves propagate through saturated porous materials. We use a rotated-staggered-grid finite difference modeling scheme to simulate elastic wave phenomena in a digitized 2D structural model obtained from micrographs of a loose beach sand. When considering ultrasonic wave propagation wave in models with explicit inclusion of granular structure, the heterogeneities of quartz and pores in size and shape lead to frequency-dependent seismic phenomena. By comparing the numerical results from models where three sources with different frequencies were used, we saw that (1) strong particle motions concentrate mostly in fluid; (2) significant variations in pressure are observed in the fluid; (3) during the dynamic process of wave propagation, relative particle motion of the fluid and solid phases induces stress concentration on the sharp tips and corner of grains; (4) coherent particle motion is generated by sources with low frequency content, while sources with higher frequencies induce disordered particle motions. Corresponding to these particle motions, less scattered energy is observed in cases with more coherent particle motion, and strong scattering is generated by disordered particle motion.

Then we extend our work to a 3D digitized Fontainebleau sandstone sample. Though the size of the sample is small, we still consider a relative broad source frequency band (100 kHz – 20 MHz) so as to study the frequency dependent behavior of this sample. We notice a velocity minimum occurring at some “critical frequency” (750 kHz). Above this “critical frequency”, the velocity increases with frequency; while below this frequency, velocity goes to a low frequency value – effective medium value. The transition from low frequency to high frequency behavior can be viewed as going from wave-like to ray-like propagation. We then study the fluid effect by saturating the pores with non-viscous and viscous brine and oil. The velocities for samples saturated with fluids are generally larger than those of dry sample at frequencies below the critical one, which shows the significant effect of the compressibility of fluids. While the velocities become smaller than those of dry sample at frequencies above the critical one, which shows that the density of fluids comes into play a significant role. We see little effect of viscosity of fluids on velocity. To investigate the scale effect, we first compare the result from dynamic modeling for case with source frequency of 100 kHz to that from static modeling by using finite element method on a sub-cube selected from the original sample. Then we elongate the 3D sample in one direction by repeating the original sample five times, and compare the result from this elongated one to that from the original one at source frequency of 100 kHz. Velocities for these three cases are close to each other. Smaller velocity from static modeling might be due to the higher porosity of the selected sub-cube sample.

1. Introduction

When considering the elastic properties of granular materials on the pore scale, even "homogeneous" samples exhibit a wide variety of microstructural features capable of influencing wave propagation. Materials such as quartz and clay in a rock sample can be treated as heterogeneities; pores between them can have different sizes and shapes saturated with fluids. In laboratory experiments, seismic waves

propagating at high frequencies are more sensitive to these pore-scale features. Particle motion in the fluid and solid phases controls the scattering of wavefields in this class of heterogeneous material; such scattering results in both the attenuation of seismic energy and the distortion of recorded waveforms. For porous media saturated with viscous fluids there are also at least two types of physical mechanisms that effect wave propagation: Biot's inertial mechanism (Biot, 1956) and local or squirt mechanisms (Dvorkin and Nur, 1993; Dvorkin, et al., 1995).

Finally there are scale effects due to using different acoustic frequencies (e.g., Mukerji, et al., 1995) that are sensitive to microstructures of porous media, like the size of the heterogeneities or correlation length. Recently, static and dynamic numerical models have been applied to small, digitized rock samples (~ 1 mm^3) to verify the theories developed for porous media (Arns, et al., 2002; Saenger, et al., 2005). A challenge for such modeling work is how the results obtained from such small samples can represent the laboratory or field measurements at lower frequencies. Numerical model results have been able to match theoretical predictions well in static modeling with the finite element method (Arns, et al., 2002) and dynamic modeling with the finite difference method for relative large fractured media (Saegner and Shapiro, 2002; Saenger et al., 2004)..

To study scattering, fluids and scale effects, we begin with the fundamental physics – the particle motions of the fluid and solid phases on the micro-scale. This can help us understand how seismic waves propagate through porous media, and how microstructural features can modify the signal. To explore this topic, we carried out a set of numerical experiments first with a digitized 2D image of a loose sample of beach sand and then with a 3D representation of a sample of Fontainebleau Sandstone obtained from a micro-CT image. In this paper, we will first introduce the 2D model and the method we used in our numerical modeling, and then we will analyze the results of particle motions. By analyzing the resulting waveforms, we will show the relationship between the distortion of signals and particle motions in porous media for different frequencies. Then we extend our work to the 3D digitized Fontainebleau sandstone. In a broad frequency band, we study the velocity dispersion for the sample in the dry state and saturated with non-viscous and viscous brine and oil. As for scale effect, we study the velocity of the original sample at the lowest frequency we can handle (100 kHz), and then compare the result to that obtained from static modeling by using finite element method on a sub-cube sample, and from the finite difference method applied to an elongated model with length in the x direction five times longer than the original one.

2. 2D Digitized Models

In our modeling study, we used a segmented 2D transmission micrograph of a quartz beach sand (San Gregorio, CA), shown in Figure 1. The binary model shown has dimensions of 551 x 496 samples with 2.429 x 2.429 micron pixels. Since the original sample consisted of a loose arrangement of grains epoxied to a slide, the solid phase (shown in black) is not continuous and the resulting model should be viewed as a suspension. For our modeling study we assume the grains are pure quartz with a density of 2650 kg/m^3 and bulk and shear moduli of 37 and 44 GPa respectively (Mavko, et al., 1998). We use the properties of water, with a bulk modulus of 2.2 GPa and a density of 1000 kg/m^3, for the liquid phase. The 2D models discussed do not explicitly include the effects of fluid viscosity.

3. 2D Numerical Modeling

For our numerical modeling study, we used a finite-difference solver which implemented the rotated-staggered-grid (RSG) scheme of Saenger, et al., (2000). Since the RSG approach can effectively incorporate large contrasts in material properties, the method is well-adapted for modeling the sharp interfaces between grains and the surrounding pore fluids. For computational purposes, we put water buffer zones around the 2D model (shown in Figure 2) and used a periodic boundary along z-direction. A PML (perfectly matched layer) absorbing boundary condition was used at each end of the sample. We modeled a compressional plane wave propagating in the x-direction from the left side of the sample. The resulting wavefield was sampled by one array of receivers along the edges of the model, visible as a red dotted line in Figure 2. The array at the far end measures the transmitted wavefield. The 2D sample acts like a filter

converting the incident wave into a transmitted wave, which is altered by the micro-structures and inclusions of the sample.

Since the size and shape of the quartz, pores and channels vary in different scales, it leads to frequency-dependent seismic phenomena when seismic waves travel through such media. For this reason, we considered three sources with different frequencies, equivalent wavelengths of which are in scales of the larger quartz grains, medium quartz grains, and small inter-grain channels in this sample respectively, as shown in Figure 3.

4. Relative Particle Motion

The compressional wave source travels along paths crossing water and quartz alternatively. Because water is much more compliant than quartz, the same body force can generate higher perturbations in the water as compared to the grains. As seen in Figure 4, the larger particle motions mostly concentrate in the water, which generates vigorous change of the pressure field in the water, especially at high frequency. As a result, pressure changes in the water affect the solid phase, and cause stress concentrations on the sharp tips and corners of grains. This kind of perturbation and stress concentration contribute to dynamic changes of mechanical properties of the rock sample during wave propagation. Because fluid viscosity is neglected, the narrow channels between grains do not significantly impact the wavefield snapshots in our simulations. However, we still can see that the velocity field is generally large in the channel between the two upper quartz grains (Figure 4).

In addition to the perturbation of particle motion and the concentration of the stress field, it is also interesting to look at the trend of motion of throughout the sample. As shown in Figure 4, in the case where a low frequency source is used, the particle motion maps exhibit more coherent variations; longer wavelengths average over larger regions of the sample. When we increase the center frequency of the source wavelet the motions of particles become disordered both in water and quartz.

5. Transmitted Waves

Figure 5 shows the waves received by the array located at the far side of the sample for the same experiments. From the transmitted waves shown in each figure, we can see that receivers located in the water measure high amplitudes because they directly receive pressure perturbations traveling within the fluid. At lower frequency, waveforms shows little scattered energy due to the coherent particle motions of the fluid and solid phases. At higher frequencies characterized by strong disordered particle motion, significant energy is transferred into the coda.

6. 3D Fontainbleau Sandstone

In our 3D modeling, a 3D digitized Fontainbleau sandstone is used, as shown in Figure 6. This model has dimensions of $200 \times 200 \times 200$ voxels with about $5 \times 5 \times 5$ microns/voxel. The porosity of this sample is about 7.37%. The black area in this figure represents quartz and white areas represent the pore space. The same mechanical properties for quartz as in the 2D sample are used.

7. 3D Numerical Modeling

In this modeling, we still use the finite difference method with implementation of the RSG scheme. By incorporating the general Maxwell body model into this method, we can also handle viscous fluid effects on wave propagation (Saenger, et al., 2005). We simulate a plane wave propagating in the x direction and two arrays of receivers are deployed on either side of the sample (Figure 7), which are used to calculate the effective velocities of waves traveling through this sample. We consider three types of two-phase cases: dry, brine saturated and oil saturated, the properties of which are listed in Table 1. Though the size of the sample (1 mm^3) is small, we still consider a relative broad source frequency band (100 kHz – 20 MHz) so as to study the frequency dependent behavior of this sample. One example of the

wave field during wave propagation is shown in Figure 8. This 3D snapshot shows the x component of the velocity field for the dry case at 10 MHz. We can easily see the distortion of the wavefront of the plane wave by heterogeneously distributed dry pores and irregular grains. Cases with the lowest frequency 100 kHz are modeled to study the low frequency behavior of such rock sample. As for the scale effect, we also extend our original rock sample in the x-direction by repeating the original image five times so as to obtain one rock sample with size of $1000 \times 200 \times 200$ voxels, and then carry out the same simulation on such elongated sample.

8. Results Analysis of 3D Modeling

8.1 Velocity Dispersion

Since we deployed two arrays of receivers on either side of the sample, we can use the cross-correlation method to obtain the time delay of wave propagation between each pair of corresponding receivers as shown in Figure 9a. For each case, we can obtain a travel time distribution panel as in Figure 9b, and then use the averaged travel time to estimate the velocity.

In our modeling, the ratio of the dominant wavelength of the compressional wave to the dimension of the sample decreases from 53 to 0.3 as frequency increases from 100 kHz up to 20 MHz. As shown in Figure 10, we notice a velocity minimum occurring at some "critical frequency" (750 kHz). Above this "critical frequency", the velocity increases with frequency; while below this frequency, velocity goes to a low frequency or effective medium value. The transition from low frequency to high frequency behavior can be viewed as going from wave-like to ray-like propagation. As studied by other researchers, seismic phenomena transit from the effective medium regime into that of ray theory with increasing frequency when waves propagate in heterogeneous media with relatively higher frequencies (e.g., Mukerji, et al., 1995). In our case, it shows almost the same trend of the dispersion curve with increasing frequency, which leads to the same transition from effective medium to ray theory as indicated in Figure 10, especially for the curve of the dry case where only scattering is taken into account. At higher frequencies, "path effects" determine the velocity measured, as waves try to find the fast path in 3D to propagate. At medium frequencies the longer wavelengths are perturbed by heterogeneities like empty pores, saturated pores or irregular grains, which induces stronger scattering. The velocity of wave propagation in medium frequencies is slowed down by such scattering. At lower frequencies, the waves average the whole media and go to the effective medium regime.

8.2 Fluid Effect

Observations in laboratory measurements suggest that the velocities of fluid saturated samples are generally higher than those for dry rocks, but those measurements are taken in a relatively lower frequency band like sonic or lower ultrasonic frequencies. The modeling results (Figure 10) show such fluid effect on velocity in the low frequency range (<750 kHz). As shown in Figure 10, the velocities for samples saturated with fluids are generally larger than those of dry sample at frequencies below this critical frequency, which shows the effect of the compressibility of fluids. While the velocities become smaller than those of the dry sample at frequencies above this critical frequency, which shows that the density of fluids play a significant role. We have not been able to check the results from numerical modeling with laboratory data for these high frequencies.

8.3 Scale Effect

We are also interested in looking at the propagation behavior at lower frequency because most field applications are below the kilohertz range. Due to the limits of the size of the sample and computational power, the lowest frequency we can handle on this sample is 100 kHz. For the cases saturated with non-viscous brine, we compare the velocities at 100 kHz from the original sample and the elongated one to that from the static modeling obtained by the finite element method. For the finite element modeling a sub-cube with size of $60 \times 60 \times 60$ voxels is selected from the original sample due to the limit of

computational power. Unfortunately, the porosity of the selected sub-cube is about 11.3%, which higher than the full size sample used in the finite difference modeling. The results for the three difference models are listed in Table 2. First, we can see that for the dynamic modeling with the finite difference method at 100 kHz, the velocities of the compressional wave for the original and elongated samples are close to each other, which shows the size of the model has little effect on the velocity for the sample saturated with non-viscous brine. Second, the velocity estimated from the static modeling is smaller than those from the dynamic modeling. There might be two factors contributing to this difference: (1) the sub-cube used for the static modeling has higher porosity, which can cause the smaller velocity once it is fully saturated with brine; (2) even though 100 kHz is the lowest frequency in the dynamic modeling, it is still a high frequency compared to that in static modeling where zero frequency is considered. As shown in the velocity dispersion curve in Figure 10, velocity could increase with frequency. However, we believe that the effect of velocity dispersion on such a small sample, even at 100 kHz, will not contribute to the velocity difference significantly since the wavelength of a wave at 100 kHz is about 53 times the dimension of the original sample. Therefore, the porosity difference probably plays the most important role in this case.

9 Conclusions

Our numerical study in 2D has first demonstrated the relationship between particle motions of fluid and solid and signals received when a compressional wave propagates through a saturated porous media. Due to the heterogeneities of quartz and pores in size and shape, frequency-dependent seismic phenomena are observed. Sources with lower frequencies induce coherent particle motions and generate less scattered energy, while higher frequencies cause disordered particle motions and strong scattering. Particles in water generally have higher perturbation leading to larger variations in the pressure field, which reacts on quartz and causes stress concentration on sharp tips and corners dynamically.

In the 3D modeling on the digitized Fontainbleau sandstone, we investigate the frequency dependent features of the velocity – velocity dispersion. In the broad frequency band considered (100 kHz – 20 MHz), we notice a velocity minimum occurring at some "critical frequency" (750 kHz). Above this "critical frequency", the velocity increases with frequency; while below this frequency, the velocity goes to a low frequency or effective medium value. The transition from low frequency to high frequency behavior can be viewed as going from wave-like to ray-like propagation where "path effects" come play an important role in wave propagation. The velocities for samples saturated with fluids are generally larger than those of dry sample at frequencies below the critical frequency, which shows the significant effect of the compressibility of fluids. The velocities become smaller than those of the dry sample at frequencies above the critical one, which shows that the density of fluids plays a significant role. The viscosity of fluids shows little effect on the velocities, and the dominant factor is seismic scattering since we see the velocities for dry and fluids saturated cases almost follow the same dispersion trend. For dynamic modeling at the low frequency end, velocities at 100 kHz for the original and elongated images are close to each other, which shows little effect of the size of the sample on velocity. These two velocities from dynamic modeling are also close to that from static modeling on a sub-cube. The velocity difference between the dynamic and static modeling might be mostly due to the higher porosity of the sub-cube where fluids play a significant role.

Acknowledgements

This work is supported by the Founding Member Consortium of the Earth Resources Laboratory at MIT and DOE award number DE-FC26-06NT42956.

References

Arns, C.H., Knackstedt, M.A., Pinczewski, W. V. and Garboczi, E.J., 2002, *Computation of linear elastic properties from microtomographic images: Methodology and agreement between theory and experiment*, Geophysics, 67 (5), 1396-1405.

Biot, M.A., 1956, *Theory of propagation of elastic waves in a fluid-saturated porous solid. I. Low frequency range and II. Higher –frequency range*, J. Acoustical Society of America., 28, 168-191.

Dvorkin, J. and Nur, A., 1993, *Dynamic poroelasticity: A unified model with the squirt and Biot mechanisms*, Geophysics, 58 (4), 524-533.

Dvorkin, J., Nolen-Hoeksema, R. and Nur, A., 1995, *The squirt-flow mechanism: Macroscopic description*, Geophysics, 59 (3), 428-438.

Mavko, G., Mukerji, T and Dvorkin, J., 1998, *The Rock Physics Handbook*, Cambridge University Press.

Mukerji, T, Mavko, G., Mujica, D. and Lucet, N, 1995, *Scale-dependent seismic velocity in heterogeneous media*, Geophysics, 60 (4), 1222-1233.

Saenger E.H., Gold N and Shapiro SA, 2000, *Modeling the propagation of elastic waves using a modified finite-difference grid*, Wave Motion, 31 (1): 77-92.

Saenger, E.H. and Shapiro, S.A., 2002, *Effective velocities in fractured media: a numerical study using the rotated staggered finite-difference grid*, Geophyical Prospecting, 50, 183-194.

Saenger, E.H., Kruger, O.S. and Shapiro, S.A., 2004, *Effective elastic properties of randomly fracutred soils: 3D numerical experiments*, Geophysical Prospecting, 52, 183-195.

Saenger, E.H. and Shapiro, S.A., 2005, *Seismic effects of viscous Biot-coupling: Finite difference simulations on micro-scale*, Geophysical Research Letters, 32, L14310, doi:10.1029/2005GL023222.

Table 1: Properties of materials for cases modeled

Quartz	Vp = 6000 m/s, Vs = 4070 m/s, Den = 2650 kg/m3				
Pores	Dry	Brine		Oil	
	Vp = 0 m/s Vs = 0 m/s Den = 10^{-4} kg/m^3	Vp = 1700 m/s Vs = 0 m/s Den = 1000 kg/ m^3		Vp = 1440 m/s Vs = 0 m/s Den = 810 kg/ m^3	
		Viscosity (Pa.s)		Viscosity (Pa.s)	
		0.0	0.001	0.0	5

Table 2: Comparison of velocity of the dynamic and static modeling for case saturated with non-viscous brine.

	FDM (f = 100 kHz)		FEM (f = 0 Hz)
	Original[1]	Elongated[2]	Smaller[3]
Vp (m/s)	5430	5440	5200

1. Original sample: $200 \times 200 \times 200$ voxels, porosity 7.37%
2. Elongated sample: $1000 \times 200 \times 200$ voxels, porosity 7.37%
3. Smaller sample: $60 \times 60 \times 60$ voxels, porosity 11.3%

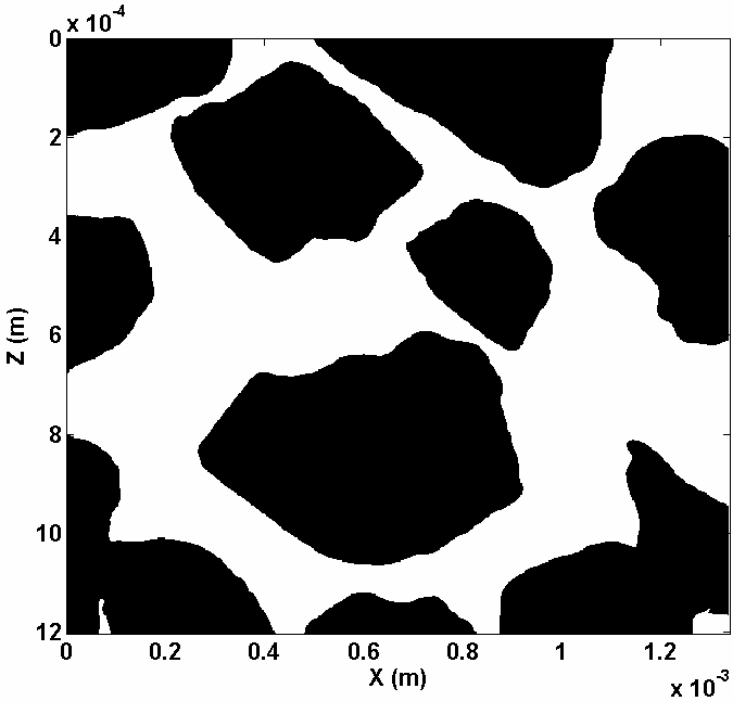

Figure 1: A segmented 2D image of a quartz sand sample (San Gregorio, CA). The quartz grains are shown in black. In our simulations, the grains assumed to be suspended in water.

Figure 2: The geometry of our numerical experiment in 2D. A compressional plane wave propagates through the sample from left. One array of receivers (red dotted line) samples the incoming wavefield.

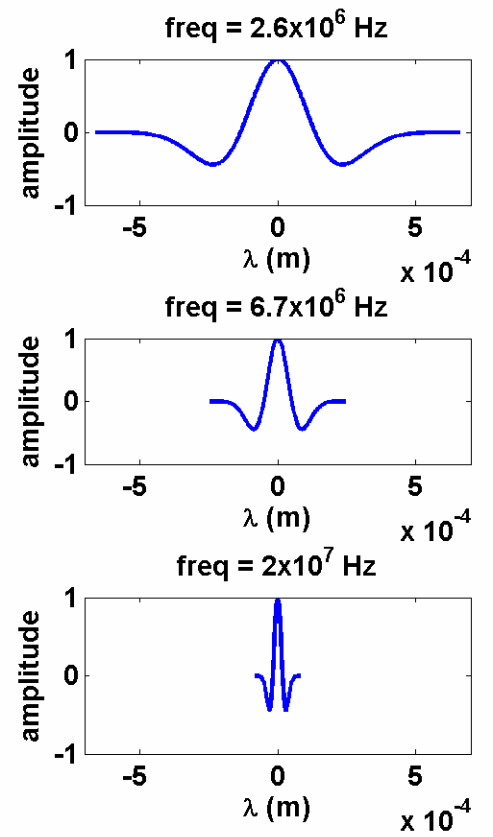

Figure 3: Three sources with different frequencies are used in numerical modeling. The lowest frequency wavelet has an equivalent wavelength similar to that of the largest grain in the image while the highest frequency source one has a wavelength on the order of the smallest channel dimension.

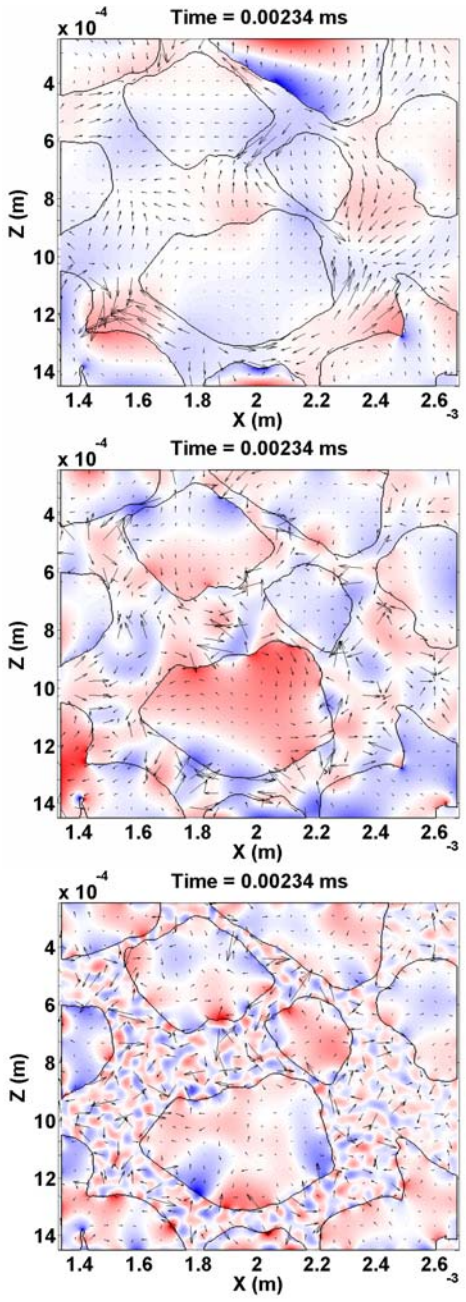

Figure 4: Snapshots for pressure and velocity fields for three cases in which source has different frequency. Color background shows the magnitude of pressure field: blue represents extension and red represents compression. Arrows show the magnitude of the velocity of particle motion. The concentration of stress at sharp tips and corner is particularly visible at for the two cases with lower frequency wavelets. From low to high frequency, particle motions become disordered, and perturbations in water contribute mostly to energy scattering.

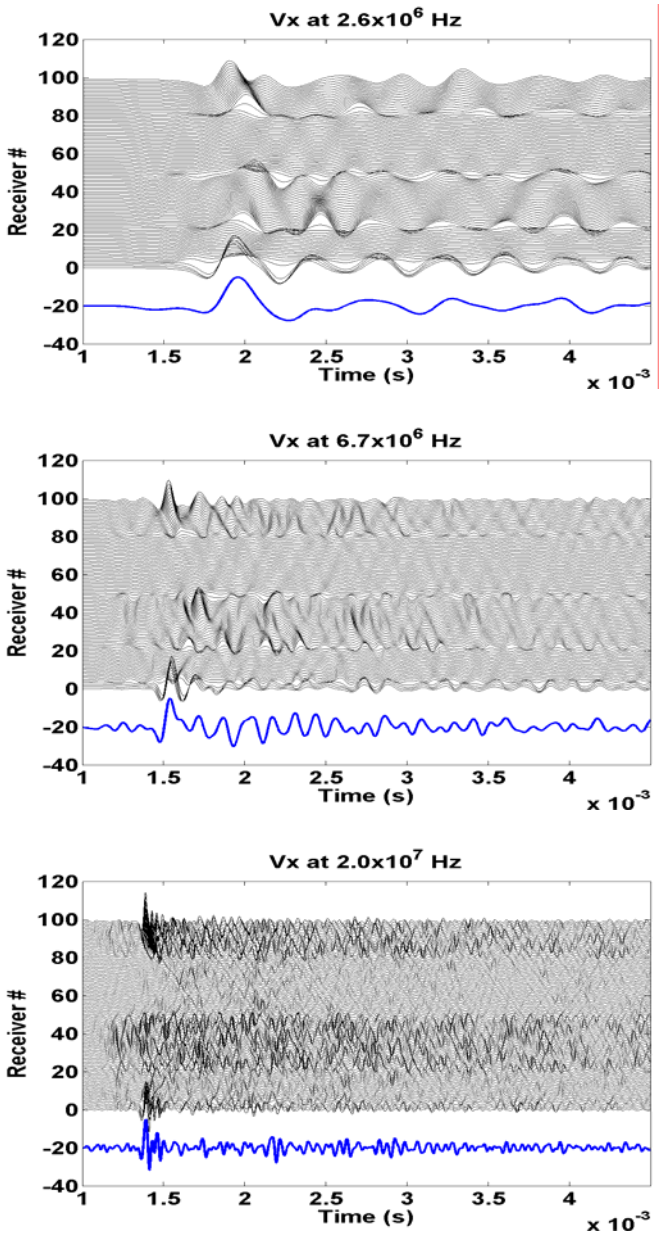

Figure 5: Transmitted seismic waveforms for three cases in which source has different frequencies. With the frequency increases, the scattered energy becomes strong because of the strong disordered particle motions. The blue curve in each figure is the stacked trace.

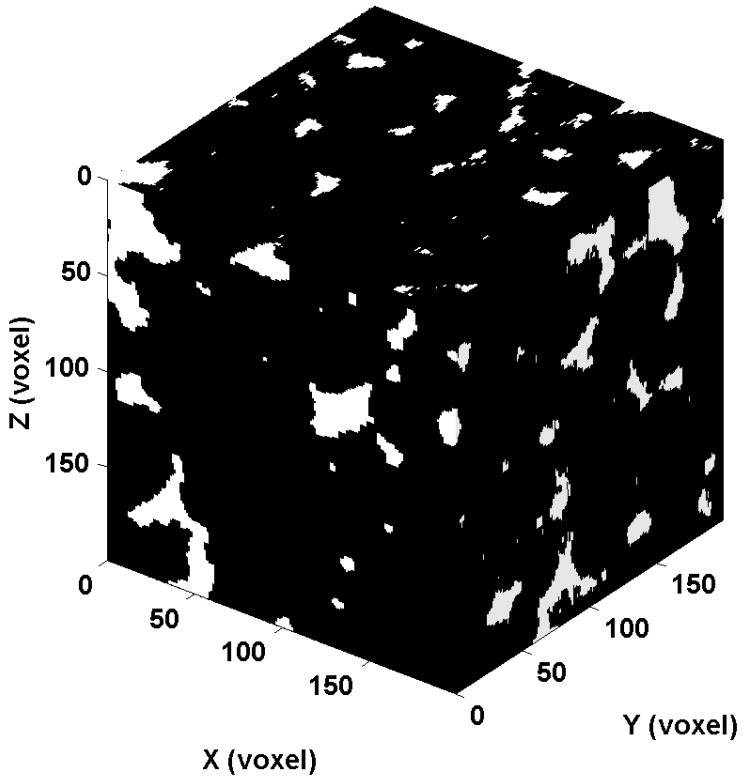

Figure 6: A 3D digitized Fontainebleau sandstone. The quartz grains are shown in black while the pore spaces are shown in white.

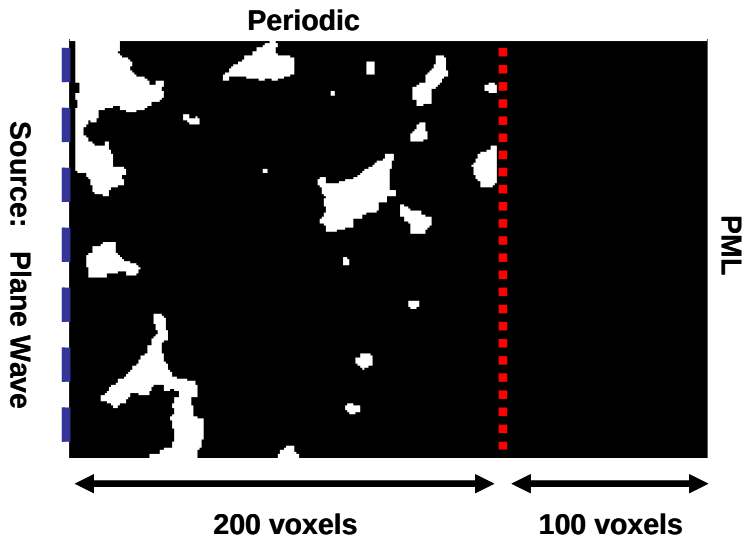

Figure 7: The geometry of our numerical experiment on 3D sample. A compressional plane wave propagates through the sample from left. Two arrays of receivers (blue dash line and red dotted line) sample the incoming wavefield.

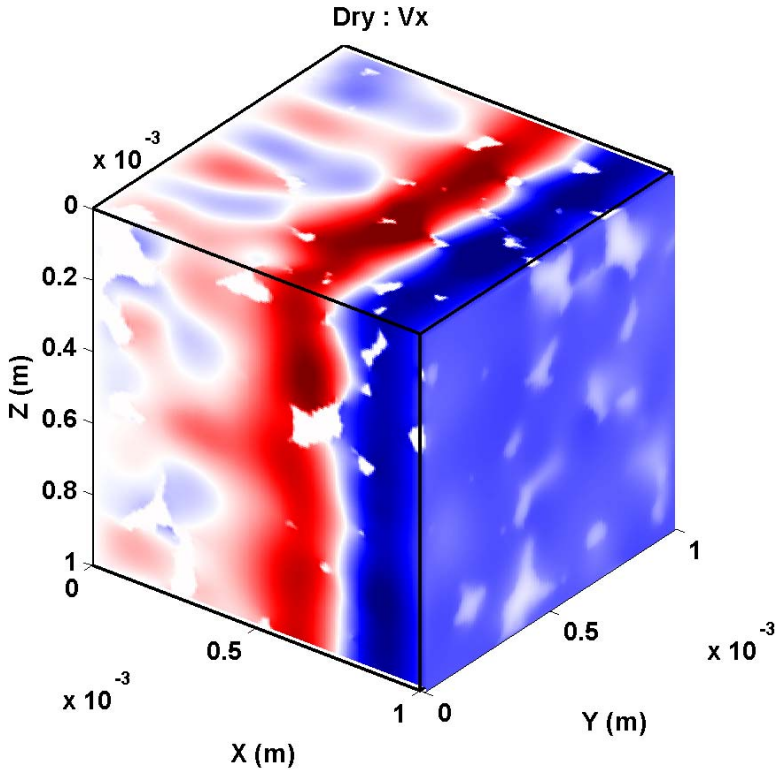

Figure 8: 3D snapshot of x component of velocity field for dry case at 10 MHz.

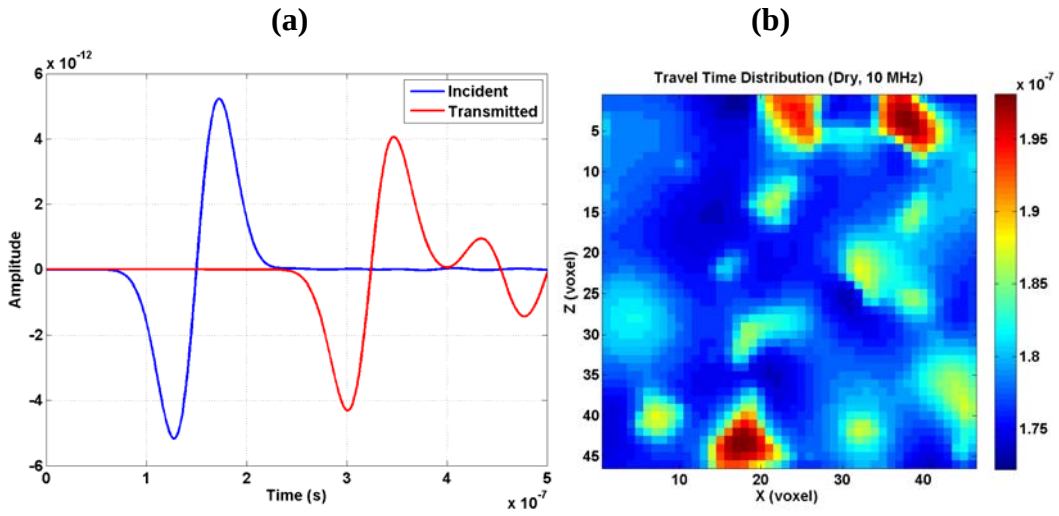

Figure 9: (a) Seismic traces for one receiver pair; (b) Travel time distribution calculated from cross-correlation method on receiver pairs.

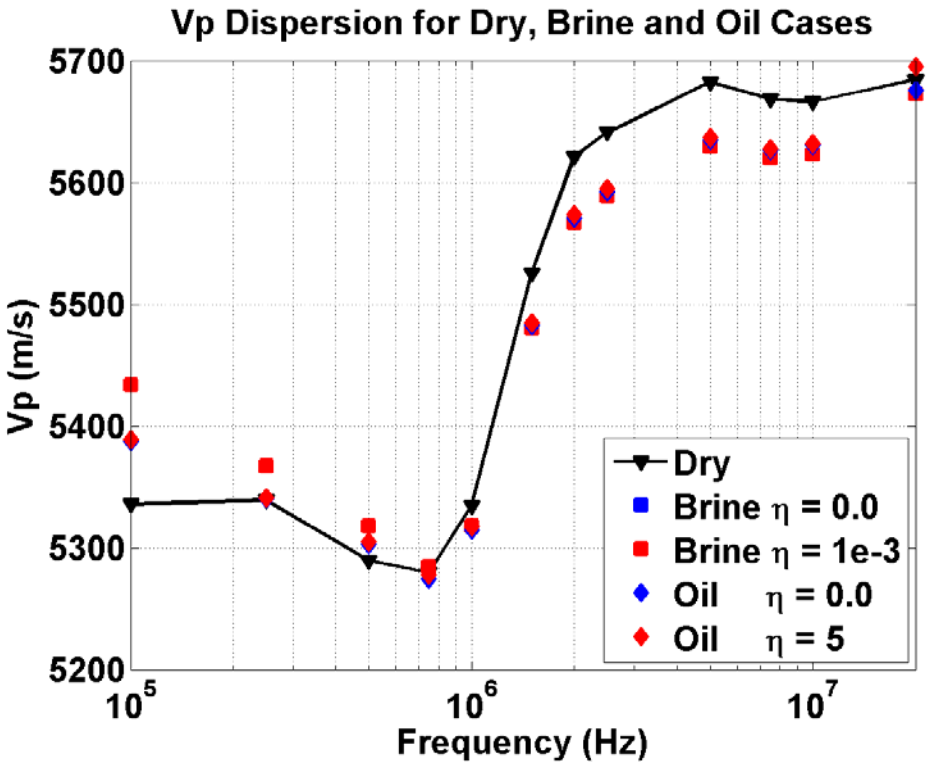

Figure 10: Velocity dispersion curves for cases saturated with dry, brine and oil.